Dynamics of a Two-Dimensional Flow Subject to Electromagnetic Forces

L. M. Moubarak and G. Y. Antar[1]
Physics Department, American University of Beirut, Riad El-Solh, Beirut 1107 2020, Lebanon[a)]

(Dated: 15 April 2011)

A novel experimental setup designed to study the dynamics of two-dimensional (2D) structures is presented. It consists of a square container filled with a thin layer of a conducting electrolyte solution, namely potassium hydroxide. With permanent magnets creating an axial magnetic field and a set of electrodes of alternating polarity distributed around the edges of the container, we generate coherent primary vortices. Farther from the edge, secondary vortices are observed driven by the primary ones and because the fluid used is viscous. We report the onset of self-generated jets heading from one corner towards the center of the container. We show that they are a consequence of vorticity induced by the magnetic field gradient interacting with the primary and secondary edge vortices. Consequently, the latter are observed to go through a vortex merging process because of this *gradB* perturbation. A stationary regime is achieved 60 seconds from turning the electric current with correlation functions reflecting the coherent modes in the flow.

PACS numbers: 52.30.Cv, 47.27.De, 47.32.cb, 47.63.mf
Keywords: magnetohydrodynamic, coherent vortices, two-dimensional turbulence

[a)]Electronic mail: ghassan.antar@aub.edu.lb

I. INTRODUCTION

Two-dimensional (2D) turbulence is the focus of a large number of studies for fundamental reasons where a good knowledge of this phenomenon is still needed and for its wide applications in many important areas like fusion plasmas and geophysics. In nuclear magnetic fusion reactors[1], it is necessary to confine the particles for a certain time in order to achieve fusion. The measurements done at the edge of the confined region shows that the particles are quivering toward the walls. This anomalous transport is done by 2D turbulence and reduces the energy confinement in nuclear fusion reactors. Therefore, the understanding of 2D turbulence is a key issue to overcoming and controlling this anomalous transport in order to increase the efficiency of these machines to produce future energy. On the other hand, several phenomena observed in the atmosphere and the oceans, such as the inverse energy cascade, can be reproduced and studied in simple laboratory experiments [2]. These experiments provide, thus, a necessary tool to develop models that replicate some properties of the atmospheric and oceanic activities for a better prediction of the climate changes as it was done in Ref.[3,4].

In the past, various experimental setups were built to study 2D turbulence using mainly two types of fluids: soap films and electrically conducting solutions. In soap films, Couder *et al.* visualized 2D turbulence using a grid of cylinders across a horizontal flow and vortex merging was observed and characterized[5,6]. Later on, advanced techniques were designed leading to precise velocity and vorticity measurements[7,8]. In electrically conducting solutions, such as liquid metals and electrolytes, 2D vortices were generated by the Lorentz force. The magnetic field suppresses the velocity fluctuations in the direction parallel the field lines which results in 2D flow[9,10]. In this context, Sommeria *et al.*[2] studied the dynamics of a thin layer of the liquid mercury in a square container in the presence of an alternating horizontal electric field and a strong axial magnetic field. Energy spectra showing the inverse cascade as well as vortex merging were observed in these experiments. Another setup was built to investigate 2D turbulence using electrolytes where a unidirectional electric current was driven from one side of a square or rectangular container to the other, in the presence of an axial magnetic field created by an array of permanent magnets fixed from below. These

containers were filled with two layers of conducting solutions with different densities and the stratification at the interface enhances the vertical momentum transfer resulting in a 2D flow in the upper layer. The alternation of upward and downward magnetic field lines with the unidirectional electric field create an array of coherent vortices covering the surface of the flow as long as the current is turned on. After shutting it down, a quantitative analysis of the decaying regime was performed as a function of time[11,12]. The power laws found experimentally were consistent with the results obtained numerically[13]. The inverse energy cascade which was experimentally studied in[2] for the first time, was later observed in a system which satisfies stationarity, homogeneity and isotropy [14]. A 2D enstrophy cascade was also observed experimentally in Ref.[15]. In addition to the study of coherent vortices in a decaying and in a forced system, the study of dynamic jets generated within the flow was done in[16]. Practically, the permanent magnets were assembled below a rectangular container with different arrangements and by changing the direction of the electric current with respect to the sides of the container, different types of jets were produced.

We present in this paper a new experiment to generate 2D coherent structures and to investigate their 2D properties. We describe the experimental setup and discuss the dynamics of the flow. The experiment shows that coherent vortices are generated near the edge of the container, as expected. These are called primary vortices. Further away from the edges, secondary vortices of different size are observed. We are able to fully explain the onset of jets and reveal the role of the magnetic field gradient in generating vorticity.

II. THE EXPERIMENTAL SETUP

The square container shown in Fig. 1 is a 25×25 cm box made of electrically non-conducting Plexiglas plates. On each one of the four walls, 13 stainless steel electrodes, of length 16 cm each, are inserted with alternating polarity. The distance between two consecutive electrodes is 2 cm. They are connected in parallel to a DC power supply. Consequently, the electric field strength between each two consecutive electrodes is the same, but the direction is inverted when going from one couple of electrodes to the following.

The electrolyte used in our experiments is a Potassium Hydroxide (KOH) solution with

a concentration is 27% of water mass where the solution is at its maximum conductivity of approximately 550 Siemens/m[17]. The viscosity of the KOH solution is about that of water.

Below the container, 33 Neodymium permanent bar magnets of size $7.62 \times 1.27 \times 0.64$ cm are inserted in three adjacent drawers each having 11 magnets and fit below the container as it is shown in Fig. 1. The distance between two consecutive magnets is 1 cm in the x and y directions. Because of the distribution of the magnet bars, a spatially variable axial magnetic field is produced at the container surface. The magnetic field was measured using a Tesla-meter probe which measures the intensity of the magnetic field based on Hall Effect. Fig. 2(a) and (b) illustrates the axial magnetic field as a function of x and y for several values of y's and x's respectively. The positive values indicate a constant magnetic field direction whereas the amplitude changes. In the x-direction, strong magnetic field gradient is reported in the region between the drawers and the gradient, assessed to be about 1 T/m. In the y-direction, on the other hand, the set of discrete bars lead to a small amplitude oscillation in the magnetic field strength.

In order to diagnose the flow, we use two complementary methods. According to the first, a green dye emitting in the range 0.515 μm is dropped in the solution and a uniform white light source is used. The dye can be dropped at various times and various locations during the experiment and this can yield several information about the dynamics of the flow at different times. The other method is similar to Particle Tracking Velocimetry (PTV) technique[18] where glass beads are distributed in a homogeneous fashion in the electrolyte solution. By inserting a cylindrical lens in front of a green laser, a laser sheet of thickness 2 mm is formed in order to illuminate the flow. The sheet crosses the solution at approximately half the depth of the electrolyte solution. The reflected light is captured using the FC13 digital camera fixed above the container. It records images up to 10 frames/second at 2048×1536 pixels. Since the whole container is imaged we obtain a spatial resolution of 0.16×0.12 mm.

III. THE FORMATION OF PRIMARY VORTICES

The solution is composed of positive K^+ and negative OH^- ions of equal concentration. In order to illustrate the generation of primary vortices, we draw in Fig. 3 four electrodes

and the consequent three electric fields, $\vec{E}$, with alternating directions in the presence of an axial magnetic field, $\vec{B}$, pointing out of the page. The Lorentz force is responsible for the motion near the walls leading to the fluid acceleration. The Navier-Stokes equation is

$$\rho\frac{\partial\vec{v}}{\partial t} = -\vec{\nabla}p + \vec{j}\times\vec{B} + \mu\triangle\vec{v} \tag{1}$$

with $\vec{j}$ being the electric current density given by Ohm's law

$$\vec{j} = \sigma(\vec{E} + \vec{v}\times\vec{B}). \tag{2}$$

The fluid density is ρ, σ is the solution electric conductivity, p is the fluid pressure, $\vec{v}$ is the velocity field, $\vec{E}$ is the applied electric field with components $(E_x, E_y, 0)$ and $\vec{B}$ is the magnetic field $\vec{B} = (0, 0, B)$. At one boundary, we have $E_x = 0$ and neglecting the pressure gradient and viscosity, one can rather easily show that, for small Reynolds numbers, one has the solution

$$v_x(t) = \frac{E_y}{B}(1 - \exp(-t/\tau)), \quad \text{where} \quad \tau = \frac{\sigma B^2}{\rho}.$$

Consequently, a typical time for the increase of the velocity is of the order of 10 ms. Of course the velocity will not increase to reach $E_y/B \simeq 100$ m/s since non-linear effects and the drag of the fluid that needs to be moved will bring the end velocity down to about few centimeters per second. By alternating the direction of the electric field while preserving the direction of the magnetic field, we create a velocity field towards the container wall at some places and away from it at others. Extending this analysis to the rest of the container, we find that consecutive vortices are expected to circulate in opposite directions near the wall.

Experimentally, the onset of vortical motion was recorded with the container filled with a layer of KOH solution of depth 1 cm. A potential difference of 2.5 V is applied across each couple of electrodes driving in the solution a total current of 1 A. The experiment was done using the dye as a tracer and was recorded using the FC13 fast imaging camera capturing at the rate of 5 frames per second. The procedure started by one drop of dye at one side of the container which is then left to diffuse creating a rather large spot with diameter about the distance between two electrodes as it is shown in Fig. 4(a). The current

is then turned on and the evolution of the flow in front of the electrodes is recorded. In (b), taken 2 seconds after the current is turned on, the motion in front of the electrodes is visible where in between the electrodes, the dye is pushed away from the edge of the container while outside it is pulled towards the edge. This is in agreement with Fig. 3 and the theoretical predictions that we have discussed above. In (c) and (d), one can identify the two counter-rotating vortices which start to change shape as a consequence of the non-linear interaction among neighboring vortices; this aspect can be seen in Fig. 3(e) to (h) where the vortex pair is deformed.

IV. SECONDARY VORTICES

Away from the edge of the container, where primary vortices are driven by the Lorenz force, another succession of vortices are observed. The electric field is strongest at the edge of the container where the distance between electrode is the shortest. As the flow is viscous, momentum is transported to regions far from the wall causing the onset of secondary vortices. They can be observed in Fig. 5 forming a raw parallel and counter-rotating with respect to the primary vortices. The size of the secondary vortices is about the same as the primary ones but they are seen to circulate at lower speed.

V. SELF-GENERATED JETS

The dye is dropped at one corner and its motion is recorded as it is transported by at first primary vortices. To our surprise, it is observed that the primary vortices have disappeared and the dye is pushed from a corner towards the center of the container at relatively a high speed. Fig. 6 shows consecutive images where the dye, instead of remaining near the container edge transported by primary vortices, it is directed to the center of the container in the form of a coherent diagonal jet. In this section, we describe the formation process of these 'self-generated' diagonal jets. In Fig. 6(a) we see the row of primary vortices close to the container edge are nearly absent especially close to the top-right corner. In (b) the jet starts to be visible as the dye is transported towards the middle of the container and

this aspect is clearer in (c), (d) and (e). The propagation speed of the dye is estimated to be about 5 cm/s. However, from sub-plots (e) to (h), the jet seems to stop and the dye is diverted to the right and the left. We shall show that the formation process of this jet is rather complex, caused initially by what we call a $gradB$ jet with dynamics coupled to edge vortices modifying the latter. This explains the lack of primary vortices near the top-right corner giving rise to two diagonal jets in opposite directions which explains why the jet in Fig. 6 stops in the middle of the container.

A. Phase I: $gradB$ Jets

To unveil the onset of the diagonal jet, we performed an experiment where we first let the dye cover the entire surface of the container. When the current is on, two jets parallel to each others are observed. They move in the y-direction from one side of the container to the other as shown in Fig. 7 which displays their evolution at different times. Fig. 7(a), taken 10 s after the current is switched on, shows that the jets are still absent and only vortices are generated at the container edges. Fig. 7(b) is taken 5 s later, that is 15 s after the power is on, clearly shows two parallel jets moving the dye in the y-direction. Fig. 7(c) shows that they affect a larger area before they start to deform in (d) because of their interaction with primary and secondary vortices.

The two parallel jets are formed above the space between adjacent drawers below the container. The absence of a magnetic field as shown earlier in Fig. 2 creates there a strong magnetic field gradient of about $\partial_x B \simeq 1$ T/m. It is rather well-known in plasma physics that despite the explicit absence of the magnetic gradient in the magnetohydrodynamic equations, it plays nevertheless a role similar to the pressure gradient[19]. In order to show this effect from a purely neutral fluid dynamics point of view, let us consider the Navier-Stokes equation in 2D. Since we are analyzing the onset of these structures, the non-linear term is neglected. Far from the container edge, we have $\vec{E} = E_x\hat{x} + E_y\hat{y} + 0\hat{z}$ where now the two components of the applied electric field may be of the same order. Eq. 1 is projected on the x and y-directions and in order to remove the pressure gradient term, we take the partial derivative of Eq. 1 with respect to y and subtract it from the partial derivative of

Eq. 1 according to x. The resultant equation is that for vorticity where

$$\rho\frac{\partial\omega}{\partial t} = \sigma B(\partial_x E_x + \partial_y E_y) + \sigma(E_y\partial_y B + E_x\partial_x B) - \sigma B^2\omega \tag{3}$$

This equation shows that vorticity is dissipated by a strong magnetic field but it is generated by gradients in either the electric or the magnetic field. The gradient of the axial magnetic field gradient in the x-direction is almost 10 times stronger than the gradient in the y-direction, as it can be deduced from Fig. 2(a) and (b). Consequently, the dominant term in vorticity generation is $\sigma E_x\partial_x B$. The magnetic field dip in the x-direction leads to a gradient which has a positive and a negative parts driving vorticity in opposite directions, thus generating counter-rotating structures. This is illustrated in the sketch of Fig. 8 where we emphasize that in the region where the magnetic field is zero, the two counter-rotating vortices lead to fluid motion in the same y-direction. Extending this analysis to several magnets, a succession of opposite and counter-rotating vortices take place in the region of strong magnetic field gradient driving a jet in the region of minimum magnetic field.

B. Phase II: Diagonal jets

The second phase in the diagonal jet generation is dominated by the $gradB$ jet interaction with secondary and primary vortices. As it can be seen in Fig. 7 secondary vortices exist on both sides of the jet. In order to understand the $gradB$ jet interaction with vortices, we performed an experiment where glass beads are used as tracers and the illumination is done with a laser sheet. A contour plot of an area that is about 11×16 cm near the upper right-hand corner of the container is determined at half the maximum light intensity. We overlay the result of several frames in order to show the trajectories of the beads as they move in time. This is shown in Fig. 9 where in (a) one of the two $gradB$ jets is seen heading from the top of the figure to its bottom along with the secondary vortices on the sides. Because of the jet interaction with the secondary vortices, these vortices start to merge resulting in a large vortex observed in Fig. 9(b). Similarly, another large vortex is formed on the right-hand side of the jet and is more visible in Fig. 9(c). The merging of the boundary vortices explains the trajectory of the dye and the apparent absence of primary vortices in Fig. 6.

Consequently, we deduce that the interaction of the $gradB$ jet with the boundary vortices leads to (1) vortex merging at the edge and (2) modification of the $gradB$ jet direction from the y direction to almost diagonal. The jet is still observed in Fig. 9(d) taken 40 seconds later which is an indicator of its persistence as a function of time.

C. The Final Flow

The final stage of the flow is illustrated in Fig. 10 which shows the whole container 4 minutes after turning the current on. The merging of the vortices with the $gradB$ jets results in large vortices near the upper right-hand and lower left-hand corners. The reason for this fact not seen on the other two corners is caused by the polarization of the electrodes there. When they are polarized to drive the flow away from the corner, they contribute to the jets formation, when they polarized to have the fluid moving towards the edge the jet is not formed. In Fig. 10 now it is clear that there are two diagonal jets moving in opposite directions and this explains why the jet in Fig. 7 did not cross the whole container.

Three types of forces are competing in our flow, viscous, Lorentz and inertial. The dimensionless numbers should give us an idea about the important players. To compare between the $\vec{j} \times \vec{B}$ electromagnetic force and the inertial force $\rho\vec{v}.(\vec{\nabla}\vec{v})$ in the momentum balance equation, the interaction parameter N, which in our case has an electric and magnetic components, is calculated :

$$N = \frac{\sigma(\Delta V)B}{\rho v^2} + \frac{\sigma B^2 L}{\rho v} \simeq 400 + 10^{-6}. \tag{4}$$

It indicates that the electrical component dominates the inertial one which on its turn dominates the magnetic component of the Lorentz force. To compare between the viscous and the electromagnetic forces which appear in the Navier-Stokes equation, the Hartmann number is calculated, which also has an electric and a magnetic components

$$Ha^2 = \frac{\vec{j} \times \vec{B}}{\mu(\Delta\vec{v})} \sim \frac{\sigma\Delta V L B}{\mu v} + \frac{\sigma B^2 L^2}{\mu} \sim 10^5 + 25 \tag{5}$$

Here, μ is the dynamic viscosity of the KOH solution considered to be that of water. Clearly the electric component of the Lorentz force dominates by far the dynamics. The Reynolds

number assesses the importance of the inertial term with respect to the viscous one

$$Re = \frac{\vec{v}.(\nabla\vec{v})}{\mu\Delta\vec{v}} \sim \frac{vL}{\nu} \sim 250 \tag{6}$$

The Reynolds is not large for the flow to be turbulent but in a range where inertial forces dominate the viscous forces and where the flow would record complex motion.

VI. THE STATISTICAL PROPERTIES OF THE FLOW

A. Determining the Velocity Field

Now that we described and explained the flow's dynamics in our setup, we aim in this section to characterizing this evolution in a statistical fashion by accounting for the dynamics of the flow mixing boundary to core dynamics. For this purpose, we first determine the velocity field inside the container by using the spherical glass beads illuminated by the laser sheet. The velocity is obtained by following the beads light reflection from one frame to another taken at the rate of 5 frames/second. This method is quite similar to particle tracking velocimetry (PTV)[20,21]. It consists of finding the light intensity maxima in a certain region for two consecutive frames. In order for a velocity field to be defined, maxima should move a minimum of 1.5 pixels and a maximum 6 pixels in the image. The lower bound is determined after investigating a movie without beads motion and determining on the average of the light intensity fluctuations. The upper bound is determined by the flow maximum velocity. Fig. 11 shows the velocity vectors using our PTV method. The figure illustrates the overlay of several consecutive contours, at half maximum intensity, along with the velocity obtained from PTV. Excellent agreement is obtained between the two methods. Nevertheless, there exist errors which are mainly caused by the appearance and disappearance of glass beads as they slowly sediment towards the bottom, hence, moving into the laser sheet when coming from the top layers and out of it when going to the bottom. We assessed the number of maxima which appears and disappears by recording the flow without the electric current and found that only 5% might undergo this change.

B. Correlation Functions and Stationarity

Once the current is applied, the electrolyte starts to move as discussed above. The goal of this section is first to determine the correlation properties of the flow and consequently deduce the time after which the flow can be considered to be stationary. Using the x and y-components of the velocity field, we calculate the correlation functions defined as

$$C_x(\Delta x, t) = \sum_{i=1}^{N(t)} v_x(x_i, y_i, t) v_x(x_i + \Delta x, y_i, t) \ , \ C_y(\Delta y, t) = \sum_{i=1}^{N(t)} v_y(x_i, y_i, t) v_y(x_i, y_i + \Delta y, t) \ .$$

The sum is over the number of maxima in each frame which moved between two frames according to the rules described above. For velocity fields not correlated, we have $C_x = \langle v(x)v(x + \Delta x)\rangle = \langle v\rangle^2$. If the average value is subtracted from the velocity field than $C_x = 0$. On the other hand, excellent correlation leads to $C_x = \langle v^2\rangle$.

In Fig. 12(a) and (b), we plot the correlation function of v_x and v_y respectively as a function of Δx and time t. In both directions, the correlation amplitude is about zero before the current starts to flow in the KOH solution. At about 10 s, the amplitude as well as the width of the correlation start to grow in the y-direction. The total energy, determined by integrating the correlation function

$$E_x(t) = \sum_{\Delta x} \sum_{i=1}^{N(t)} v_x(x_i, y_i, t) v_x(x_i + \Delta x, y_i, t) \ , \ E_y(t) = \sum_{\Delta y} \sum_{i=1}^{N(t)} v_y(x_i, y_i, t) v_y(x_i + \Delta x, y_i, t)$$

is shown in Fig. 12(c) as a function of time. In the y-direction the E_y increases rapidly and over-shoot in a time-scale about 10 s. We interpret this over-shooting as a consequence of the *gradB* jets. Between 20 and 60 s the correlation amplitude drops slowly to reach values equal to that in the x-direction. On the other hand, we do not record this over-shoot on E_x but it rather slowly increases reaching a stationary state at $t \simeq 60$ s.

The correlation function in the y direction reflects the onset of scales smaller than 2 cm, the injection scale, with a high level of correlation and large scale structures that are about 10 and 15 cm. The latter results from the *gradB* jets and vortex merging. The coherent dynamics of the flow is reflected in the correlation function which does not show a scaling region but rather coherent modes at different length scales in both the x and y directions.

VII. CONCLUSION

We presented a study of two-dimensional coherent structures using conducting liquids subject to electromagnetic force. The electric field is generated between equally-spaced electrodes inserted at the edge of the container. The magnetic field is created by permanent neodymium bar magnets fixed below the container. When the current is turned on, coherent vortices are generated at the edge in agreement with the theoretical predictions. Since the flow is viscous, primary vortices lead to the creation of secondary vortices which are farther from the container edge. The setup of the magnets created a region with a large gradient in the axial magnetic field. It was shown that this generates vorticity and thus lead to the onset of what we call *gradB* jets. The interaction of these jets with the primary and secondary vortices lead to a modification of the jet direction and to vortex merging. We emphasize the fact that edge vortex merging is observed only where the jet perturbs the flow acting as an important factor in this process. We performed PTV on glass beads in the flow and obtained the velocity field and the spatial correlation functions. Consequently, we were able to determine the time about which stationarity is reached. The spectra of the kinetic energy did not show a scaling region but rather coherent spikes at different length scales. This is a consequence of the fact that the flow did not reach a fully turbulent regime but remains in a state where coherent vortices dominate the dynamics.

ACKNOWLEDGMENTS

This work was partly funded by the Lebanese National Counsel for Scientific Research and by the University Research Board of the American University of Beirut.

REFERENCES

[1]J. Wesson, *Tokamaks*, 3rd ed. (Oxford University Press, New York, 2004).

[2]J. Sommeria, "Experimental study of the two-dimensional inverse energy cascade in a square box," J. Fluid Mech. **170**, 139–168 (1986).

[3]V. M. Canuto, A. Howard, Y. Cheng, and M. S. Dubovikov, "Ocean turbulence: Part I, one-point closure model-momentum and heat vertical diffusivity," Journal of Physical oceanography **31** (2001).

[4]V. M. Canuto, A. Howard, Y. Cheng, and M. S. Dubovikov, "Ocean turbulence: Part II, vertical diffusivity of momentum, heat, salt, mass and passive scalars," Journal of Physical oceanography **32** (2002).

[5]Y. Couder, "The observation of a shear flow instability in a rotating system with a soap membrane," J. Physique Lett. **42**, 429 (1981).

[6]Y. Couder, "Two-dimensional grid turbulence in a thin liquid film," J.Physique Lett. **45**, 353 (1984).

[7]H. Kellay, X. Wu, and W. Goldburg, "Experiments with turbulent soap films," Phys. Rev. Lett. **74**, 3975 (1995).

[8]M. Gharib and P. Derango, "A liquid film (soap film) tunnel to study two-dimensional laminar and turbulent shear flows," Physica D **37**, 406 (1989).

[9]R. Moreau and S. Molokov, "Julius Hartmann and his followers: A review on the properties of the Hartmann layer," Fluid Mechanics and its Applications **80**, 155 (2007).

[10]J. Sommeria and R. Moreau, "Why, how, and when, m. h. d. turbulence becomes two-dimensional," J. Fluid Mech. **118**, 507 (1982).

[11]P. Tabeling, S. Burkhart, O. Cardoso, and H. Willaime, "Experimental study of freely decaying two-dimensional turbulence," Phys. Rev. Lett. **67** (1991).

[12]O. Cardoso, D. Marteau, and P. Tabeling, "Quantitative experimental study of the free decay of quasi two-dimensional turbulence," Phys. Rev. Lett. **49** (1994).

[13]G. F. Carneval, J. C. McWilliams, J. B. Weiss, and W.R.Young, Phys. Rev. Lett. **66** (1991).

[14]J. Paret and P. Tabeling, "Experimental observation of the two-dimensional inverse cascade energy," Phys. Rev. Lett. **79**, 4162 (1997).

[15]J. Paret, M.-C. Jullien, and P. Tabeling, "Vorticity statistics in the two-dimensional enstrophy cascade," Phys. Rev. Lett. **83**, 3418 (1999).

[16]J. Wells and Y. D. Afanasyev, "Decaying quasi-two-dimensional turbulence in a rectangular container: Laboratory experiments," Geophysical and Astrophysical Fluid Dynamics **98**, 1 (2004).

[17]D. M. See and R. E. White, "Temperature and concentration dependence of the specific conductivity of concentrated solution of potassium hydroxide," J. of Chem. and Eng. Data **42**, 1266 (1997).

[18]M. Raffel, C. E. Willert, S. T. Werelev, and J. Kompenhans, *Particle Image Velocimetry: A Practical Guide, (Experimental Fluid Dynamics)* (Springer-verlag, Berlin, Germany, 1998).

[19]R. J. Goldston and P. H. Rutherford, *Introduction to Plasma Physics* (Institute of Physics publishing, London, UK, 1995).

[20]W. K. B. Lüthi, A. Tsinober, "Lagrangian measurement of vorticity dynamics in turbulent flow," J. Fluid Mech. **528**, 87–118 (2005).

[21]H. X. Nicholas T. Ouellette, "A quantitative study of three-dimensional lagrangian particle tracking algorithms," Experiments in Fluids **40**, 301–313 (2006).

FIG. 1. In the left-hand image, we see a top view of the square container with the electrodes distributed at the edges. In the right-hand image, the bar magnets underneath the container in the three drawers are shown. The x and y directions are illustrated.

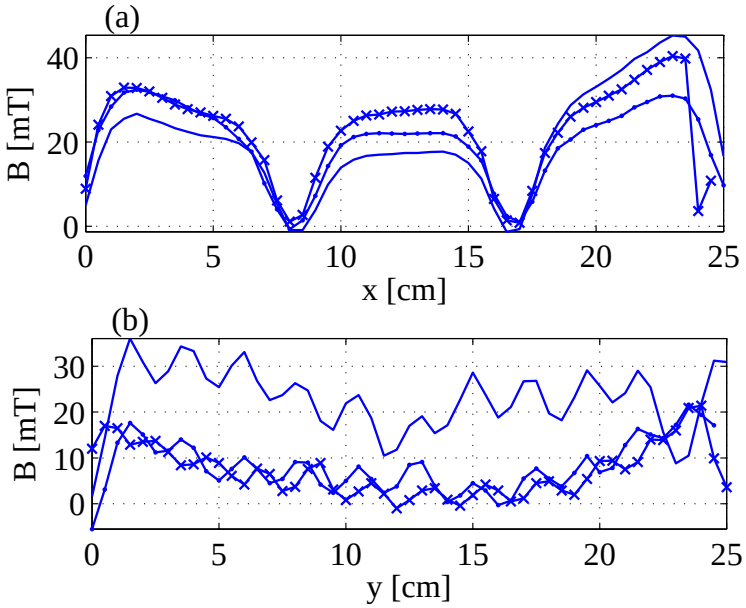

FIG. 2. Variation of the axial magnetic field in the x (a) and y (b) directions for different positions. In (b), the dots and 'x' markers represent the magnetic field strength at $x = 8$ cm and 24 cm.

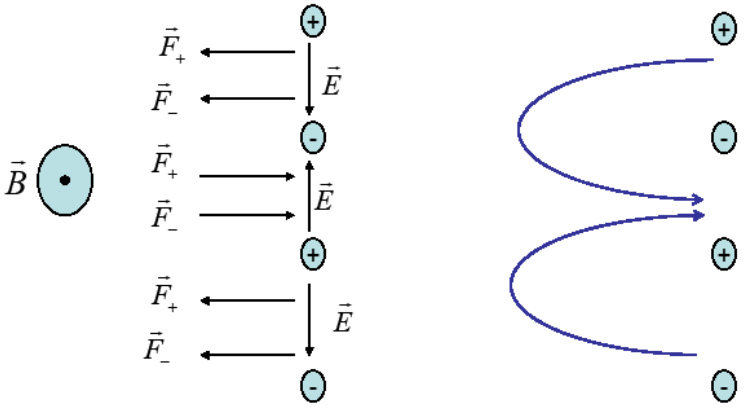

FIG. 3. Four electrodes are illustrated with the alternating electric fields in the presence of an axial magnetic field. The leftward and rightward forces result in the vortical motion shown on the right hand side. The $\vec{F_+}$ and $\vec{F_-}$ are the forces exerted on positive and negative ions respectively.

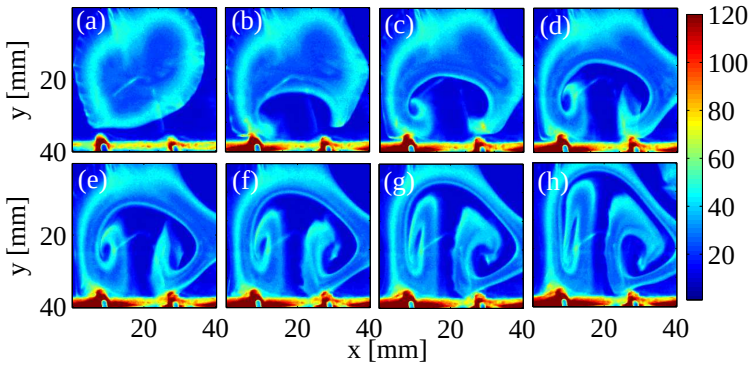

FIG. 4. The formation of a vortex pair near the edge as a function of time. In (a) it is a dye spot that was left to diffuse without the presence of an electric field. As the current is turned on, the modification of this spot shape is caused by the $\vec{j} \times \vec{B}$ velocity. The time between consecutive frames is 2 seconds. All the frames possess the same color axis.

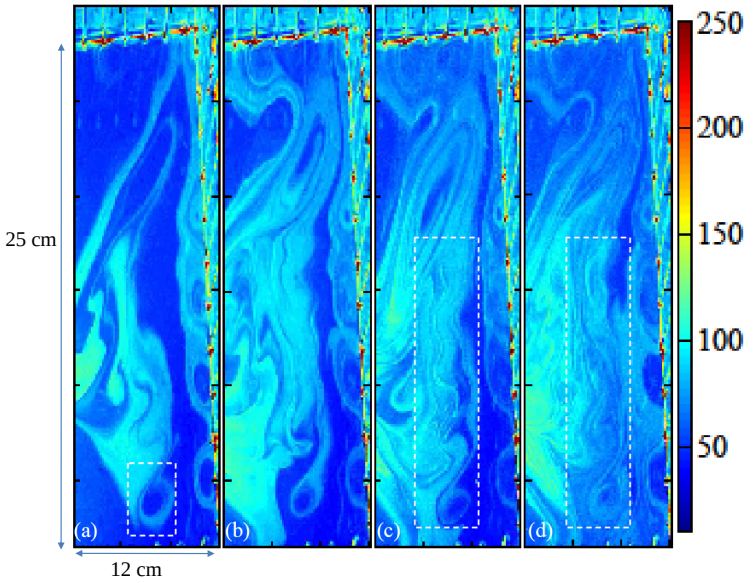

FIG. 5. The dashed rectangles indicate the location of the secondary vortices away from the edge. The time between consecutive images is 20 seconds. All the frames possess the same color axis.

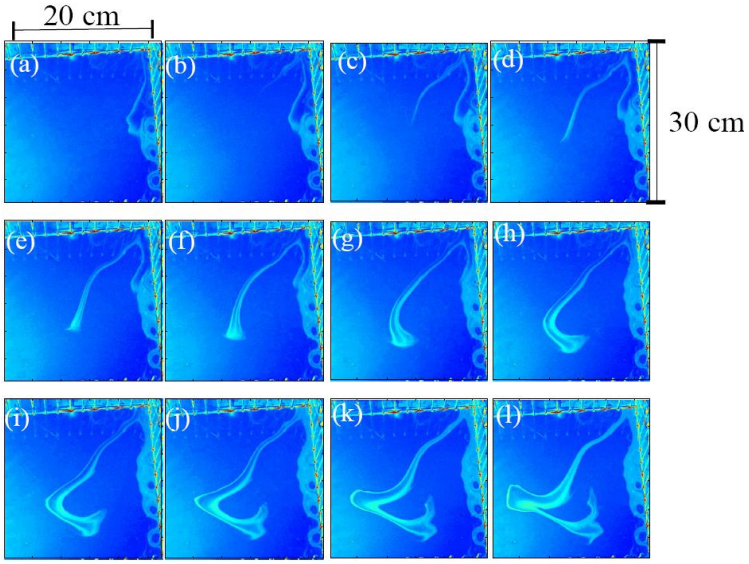

FIG. 6. Diagonal self-generated jet as it develops at the top-right corner as a function of time. In (a), one notes the absence of primary vortices and the jet is direction can be seen as the dye moves from (a) to (d). It then stops (c) to (g) and changes direction (h) to (l). The time between consecutive frames is 1 s.

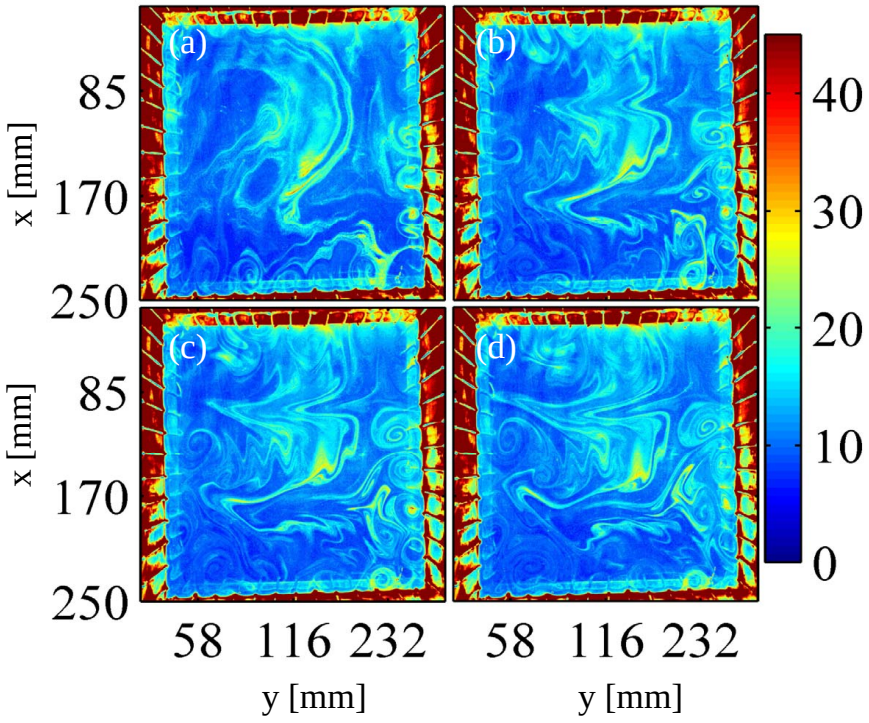

FIG. 7. The formation of the parallel *gradB* jets as a function of time. The dye was left to diffuse to fill the whole container. From (a) to (d) the images are taken at $t = 10$, 15, 20 and 25 seconds after the current is on. In (a), we point out the existence of primary vortices at the container edge. In (b), the two jets are observed as they move the dye in the x-direction. This is even clearer in (c) and in (d) we observe the interaction between these *gradB* jets and the primary and secondary vortices leading to the modification of both properties. All the images possess the same color axis.

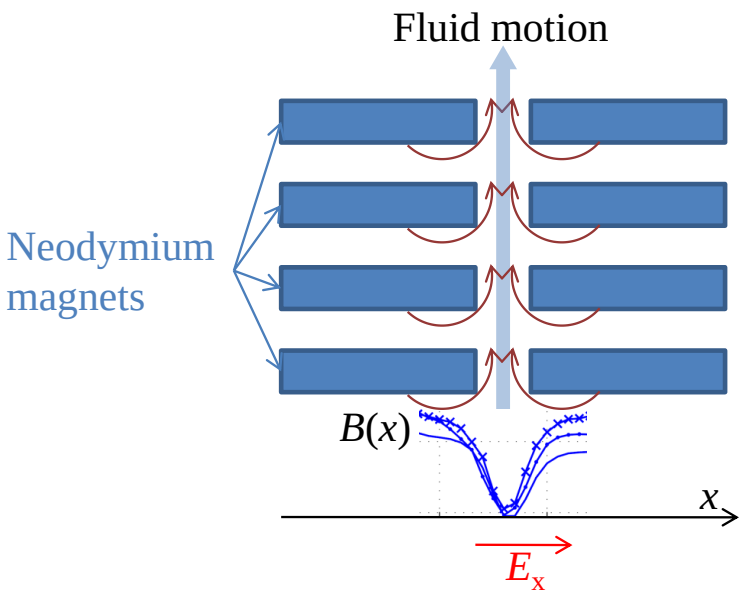

FIG. 8. In order to understand the *gradB* jet formation, we illustrate the neodymium magnets and the axial magnetic field gradient along with the electric current direction. The arrowed arcs represent the counter-rotating vortices induced by the magnetic field gradient leading to the formation of a coherent unidirectional motion as is observed by the dye.

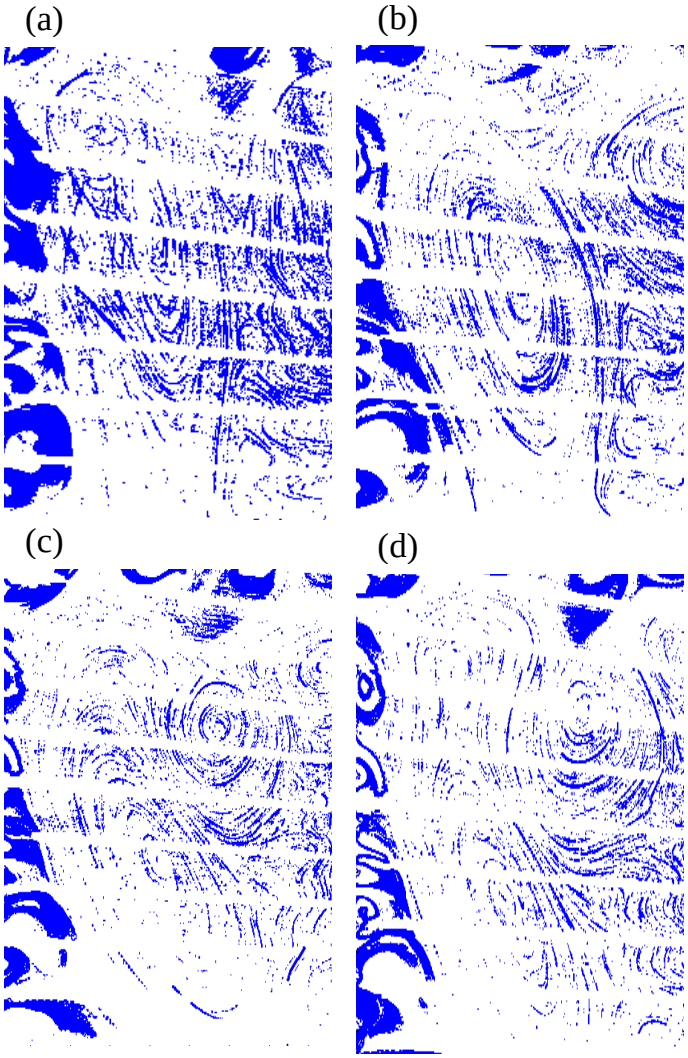

FIG. 9. The formation of a diagonal jet as a function of time is illustrated in this figure as we overlay the contour plots of 50 images at half the light intensity maxima coming from the beads. In (a), $t = 10 - 20$ s primary and secondary vortices are visible as well as the *gradB* jet. In (b) $t = 30 - 40$ s, it shows the vortex merging and the onset of one large vortex. In (c), $t = 70 - 80$ s shows the appearance of another large vortex that was hardly visible in (b) to the extreme right to form two counter-rotating vortices and the jet now is moving in the diagonal direction. in (d), we overlay between $t = 110 - 120$ s after the power is switched on and it confirms (c). The white straight lines result from the shadow of the electrodes which intercept the laser sheet.

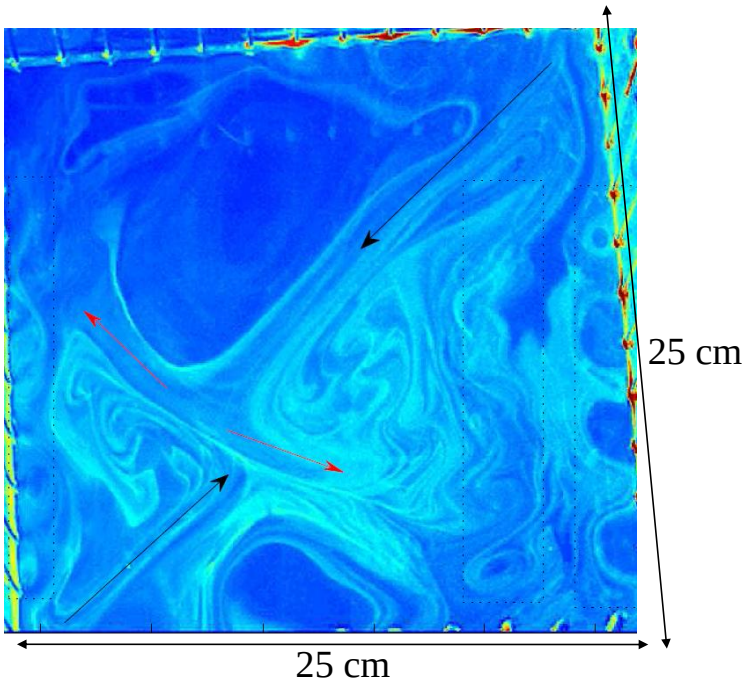

FIG. 10. This image is taken 4 minutes after the current is switched on. It gives an idea about the dynamics that are occurring inside the container. One can see the primary and secondary vortices, the two diagonal jets and the large vortices caused by vortex merging of the primary and secondary vortices as they interact with the $gradB$ jets.

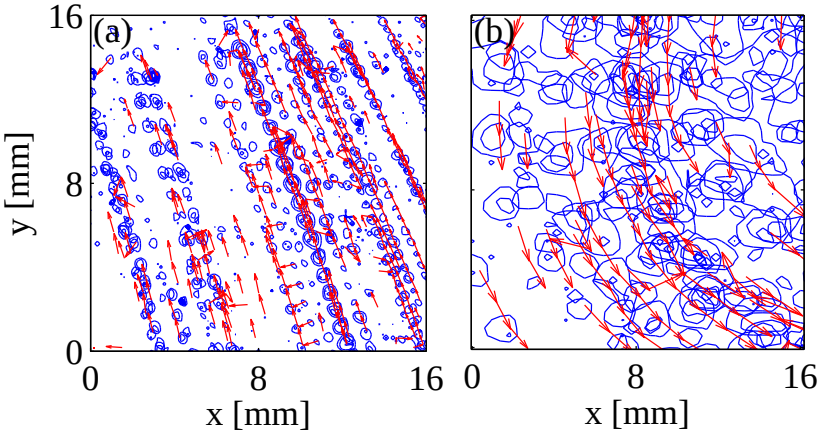

FIG. 11. We overlay the contour plots of 20 frames of the light reflection from the beads. the red arrows on the other hand represent the vectors velocity deduced from two consecutive frames. In (a), we show the velocity field for a rectilinear motion of the beads and in (b), we show the velocity field for a vortex.

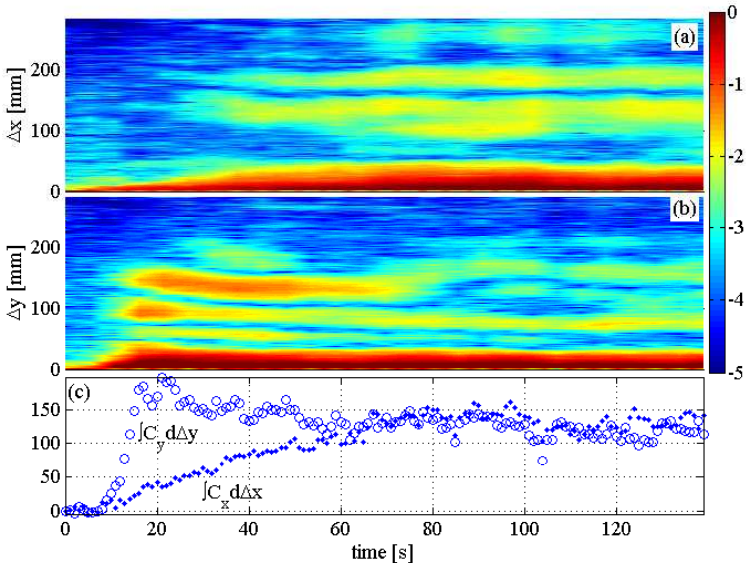

FIG. 12. The variation of the correlation function C_x as a function of Δx and time using the x component of the velocity field in (a) and the y component in (b). In (c), we plot the total correlation energy in arbitrary units as a function of time using the x, '.', and y, 'o', components of the velocity field.